Numerical solutions for thin film flow down the outside and inside of a vertical cylinder

Lisa C. Mayo[1]   Scott W. McCue[2]   Timothy J. Moroney[3]

Abstract

We consider a model for thin film flow down the outside and inside of a vertical cylinder. Our focus is the effect the curvature of the cylinder has on the gravity driven instability of the advancing contact line and to simulate the resulting fingering patterns that form due to this instability. The governing partial differential equation is fourth order with a nonlinear degenerate diffusion term that represents the stabilising effect of surface tension. We present numerical solutions obtained by implementing an efficient alternating direction implicit scheme. When compared to the problem of flow down a vertical plane, we find that increasing substrate curvature tends to increase the fingering instability for flow down the outside of the cylinder, whereas flow down the inside of the cylinder substrate curvature has the opposite effect. Further,

we demonstrate the existence of nontrivial travelling wave solutions which describe fingering patterns that propagate down the inside of a cylinder at constant speed without changing form. These solutions are perfectly analogous to those found previously for thin film flow down an inclined plane.

Subject class: 76D08, 65M06, 76E17

Keywords: thin film flow, contact line instability, viscous fingering, pattern formation

Contents

1 Introduction

The fingering pattern formed by the contact line of a thin liquid film flowing over a dry, or slightly prewetted, substrate is of significant interest to theoreticians and experimentalists alike [2, 14]. From a mathematical modelling perspective, the appropriate governing equation is typically a fourth order parabolic partial differential equation with a degenerate nonlinear diffusion term [7, 13]. The highly unstable nature of these flows makes the task of calculating accurate and efficient solutions a significant computational challenge.

In a recent study we considered the problem of thin film flow down the outside of a vertical cylinder [12]. The dimensionless model derived in that paper is

$$\frac{\partial h}{\partial t} = -\nabla \cdot \left[h^3 \nabla \left(\nabla^2 h \right) \right] - \frac{\beta}{\hat{R}^2} \nabla \cdot \left[h^3 \nabla h \right] - \frac{\partial}{\partial z} (h^3), \tag{1}$$

where the dependent variable $h(\theta, z, t)$ measures the dimensionless height of the fluid film radially from the cylinder wall, the spatial variables z and θ denote the axial and angular directions in a cylindrical coordinate system, respectively, and $\nabla = (\frac{1}{\hat{R}} \partial_\theta, \partial_z)$. The dimensionless parameter $\hat{R}$ is a scaling of the dimensional cylinder radius R with respect to the length scale $L = (\gamma H / \rho g)^{1/3}$. Here γ is the surface tension, ρ is the fluid density, g is acceleration due to gravity and H is the representative film height. The parameter $\beta = 1$ for this problem (other values of β are discussed below). A similar model for the same problem is given by Smolka and SeGall [16]. We utilise their experimental parameters for silicon oil here; they are $\gamma = 21.9\,\mathrm{dyn/cm}$, $\rho = 0.986\,\mathrm{g/cm^3}$, and $H = 0.085\,\mathrm{cm}$.

Equation (1) was derived under the assumption that $H \ll L$ to ensure the thinness of the film, but also requires that $H \ll R$. The complementary regime of flow down the outside of a narrow fibre, for which the radius of the cylinder is much less than the film thickness, was investigated in many previous studies [3, 6].

In our recent study [12], we extended the work of Smolka and SeGall [16] to produce fully three dimensional simulations and used these to confirm their linear stability analysis. The problem of thin film flow down the outside of a vertical cylinder is interesting for a further reason; it is perfectly analogous to the problem of flow down an inverted plane (that is, flow down an inclined plane making an angle $\pi/2 < \alpha < \pi$ to the horizontal) [9, 10]. Equation (1) with $\beta = 1$ is precisely the equation for flow down an inverted plane derived by Lin et al. [10], but expressed in cylindrical coordinates rather than Cartesian. This analogy occurs because $\hat{R}\theta$ is equivalent to the transverse direction on a plane. The only difference between the mathematical formulations for the two problems is that flow down the outside of a cylinder must be modelled

on a periodic domain, which implies a dependence between the parameter $\hat{R}$ and the width of the domain (specifically, the domain must be the same size as the cylinder circumference, $L_c = 2\pi\hat{R}$). This dependence between $\hat{R}$ and L_c does not apply for flow down an inverted plane. Mayo et al. [12] showed that this single difference between the two analogous problem formulations leads to very different conclusions about the stability of the contact line.

Mayo et al. [12] briefly mentioned that a value of $\beta = -1$ in (1) represents flow down the *inside* of a vertical cylinder, again under the assumption that the height of the film is much smaller than the cylinder radius. In this case, the problem is perfectly analogous to flow down an inclined plane, but one which is inclined in the range $0 < \alpha < \pi/2$ [7]. Again, like the case in which $\beta = 1$, flow on the inside of a cylinder requires $L_c = 2\pi\hat{R}$ and a periodic domain, whereas flow down an inclined plane does not.

The limit $\hat{R} \to \infty$ for both flow down the outside and inside of a cylinder corresponds to the very well studied equation for flow down a vertical plane ($\alpha = \pi/2$) [1, 4, 5, 7, 18]. By observing that $\beta = 0$ removes substrate curvature completely from the model (1), we use this value of β as a 'control' against which we compare our results for $\beta = 1$ (outside a cylinder) and -1 (inside a cylinder).

In this article we present new results for flow down the inside of a cylinder $\beta = -1$ to complement those presented by Mayo et al. [12] for $\beta = 1$. We find that substrate curvature influences the fingering patterns that form at the contact line, but in contrasting ways. Further, we present numerical evidence for the existence of nontrivial travelling wave solutions for flow down the inside of a cylinder. The travelling wave profiles consist of a fingering pattern that keeps its shape as it evolves with constant velocity. Such solutions do not exist for flow down the outside of a cylinder.

2   Numerical scheme

We employ an alternating direction implicit (ADI) scheme for the solution of (1). ADI schemes are popular solution methods for thin film type equations [10, 11, 17]. A traditional implicit approach for solving (1) requires the costly inversion of a two dimensional spatial operator at each time step of the algorithm. The advantage of an ADI scheme is that, through the approximate factorisation of this two dimensional operator, it solves the same problem via the inversion of simpler *one* dimensional operators.

Witelski and Bowen [19] reviewed and tested a number of ADI schemes for fourth order nonlinear diffusion equations . We make use of their non-iterated version of the scheme, termed pL_1 [19, Section 3.1], which derives the psuedolinear factorisation of the backward Euler method for (1):

$$\mathbf{L}_\theta w = -\delta t \left\{ \nabla \cdot \left[(h^{(n)})^3 \nabla \left(\nabla^2 h^{(n)} \right) \right] + \frac{\beta}{\hat{R}^2} \nabla \cdot \left[(h^{(n)})^3 \nabla h^{(n)} \right] + \frac{\partial}{\partial z} \left[(h^{(n)})^3 \right] \right\}$$

$$\mathbf{L}_z v = w, \quad h^{(n+1)} = h^{(n)} + v. \tag{2}$$

Equation (2) is solved in sequence at each time step in order to update the solution from $h^{(n)}$ to $h^{(n+1)}$. The linear operators $\mathbf{L}_\theta$ and $\mathbf{L}_z$ are

$$\mathbf{L}_\theta = 1 + \frac{\delta t}{\hat{R}^4} \partial_\theta \left[\left(h^{(n)} \right)^3 \left(\beta \partial_\theta + \partial_{\theta\theta\theta} \right) \right], \tag{3}$$

$$\mathbf{L}_z = 1 + \delta t \partial_z \left[\left(h^{(n)} \right)^3 \left(\frac{\beta}{\hat{R}^2} \partial_z + \partial_{zzz} \right) \right] + 3\delta t \left(h^{(n)} \right)^2 \partial_z, \tag{4}$$

and are obtained by splitting the spatial operators into distinct θ and z parts. As a result, each horizontal and vertical cross-section of the discretised domain is effectively treated as an independent one dimensional problem. These are referred to as the θ and z sweeps, respectively. The operators (3)–(4) are linearised by treating nonlinear prefactors explicitly by evaluating them at time $t^{(n)}$. We discretise $\mathbf{L}_\theta$ and $\mathbf{L}_z$ using second order finite differences on a rectangular grid. This leads to a linear pentadiagonal system for each sweep, each of which is solved efficiently with a banded solver.

The non-iterative pL_1 scheme is first order in time, and was shown by Witelski and Bowen [19] to outperform their alternative first order approximate Newton method (denoted as N_1). However, Witelski and Bowen also suggested a number of second order methods which may be implemented for further accuracy. Further, Witelski and Bowen implemented an adaptive time stepping scheme, while we take uniform steps of $\delta t = 0.01$.

To complete the problem formulation for (1), we provide boundary conditions for the edges of the computational domain. The conditions imposed along the top and bottom of the cylinder are

$$h(\theta, 0) = 1, \quad h_z(\theta, 0) = 0 \tag{5}$$

and

$$h(\theta, L_z) = b, \quad h_z(\theta, L_z) = 0, \tag{6}$$

respectively. The first condition in (5) simplifies analysis by imitating a constant source of fluid at the top of the domain, feeding the flow and encouraging finger growth. The first condition in (6) is due to the presence of a precursor film of height b prewetting the domain. This precursor film 'regularisation' avoids the well studied contact line paradox (Mayo et al. [12], and references therein, discuss related issues). We use $b = 0.07$ in this study.

The remaining two boundary conditions state that the fluid surface has zero slope in the axial direction at either end of the domain. These boundary conditions are incorporated into the model by imposing symmetry planes along the top and bottom of the discrete grid; fictitious nodes which inevitably arise in the spatial discretisation are allocated the value of their 'mirror' node from inside the domain. This treatment of the boundaries preserves second order accuracy through, for example, the discretisation $h_z \approx (h_1 - h_{-1})/(2\Delta z) = 0$, which implies that the fictitious node h_{-1} is assigned the value of the inner h_1 node.

Finally, (1) is subject to periodic boundary conditions on the lateral edges of the domain $\theta = 0$ and $2\pi\hat{R}$. These are implemented in a natural way by setting fictitious nodes to the value of nodes from the other side of the domain. The

consequence of this approach is that the θ sweep, described by the first line of (2), now produces *cyclic* pentadiagonal systems. Computational expense is minimised by using the Woodbury formula to regain regular pentadiagonal systems [15].

A 'moving window' approach was taken in the following three dimensional simulations. This arrangement shifts a small computational domain along with the moving flow front every 10 units of dimensionless time. Essentially, the algorithm is given an initial condition, the simulation is allowed to evolve to $t = 10$, and then the solution is imposed onto a new array such that the apparent contact line of the solution is shifted back towards the 'top' of the domain. The new array is then treated as the initial condition for the next simulation to $t = 10$. This method helps to centre the frame on the fingering pattern at the contact line, removing the need for a large computational domain.

3 Simulations

We begin by treating the axisymmetric version of (1):

$$\frac{\partial h}{\partial t} = -\frac{\partial}{\partial z}\left[h^3 \frac{\partial}{\partial z}\left(\beta \frac{h}{\hat{R}^2} + \frac{\partial^2 h}{\partial z^2}\right) + h^3\right]. \tag{7}$$

Mayo et al. [12] reported that ordinary travelling wave solutions exist for (7) for radii above $\hat{R} = 0.88$ when $\beta = 1$, and that the film becomes unstable to free surface waves for smaller values of $\hat{R}$. We expand on these results here.

In Figure 1 a comparison between the fluid profiles for $\beta = -1, 0, 1$ is shown for the cylinder radii $\hat{R} = 1.61, 0.88, 0.72$. In the top plot, corresponding to $\hat{R} = 1.61$, the fluid profiles for the three β cases are all quite similar, indicating that the substrate curvature effect is small at this reasonably large radius. Each of the three profiles has one main feature: a clear peak in the fluid height at the fluid front. This is referred to as a capillary ridge,
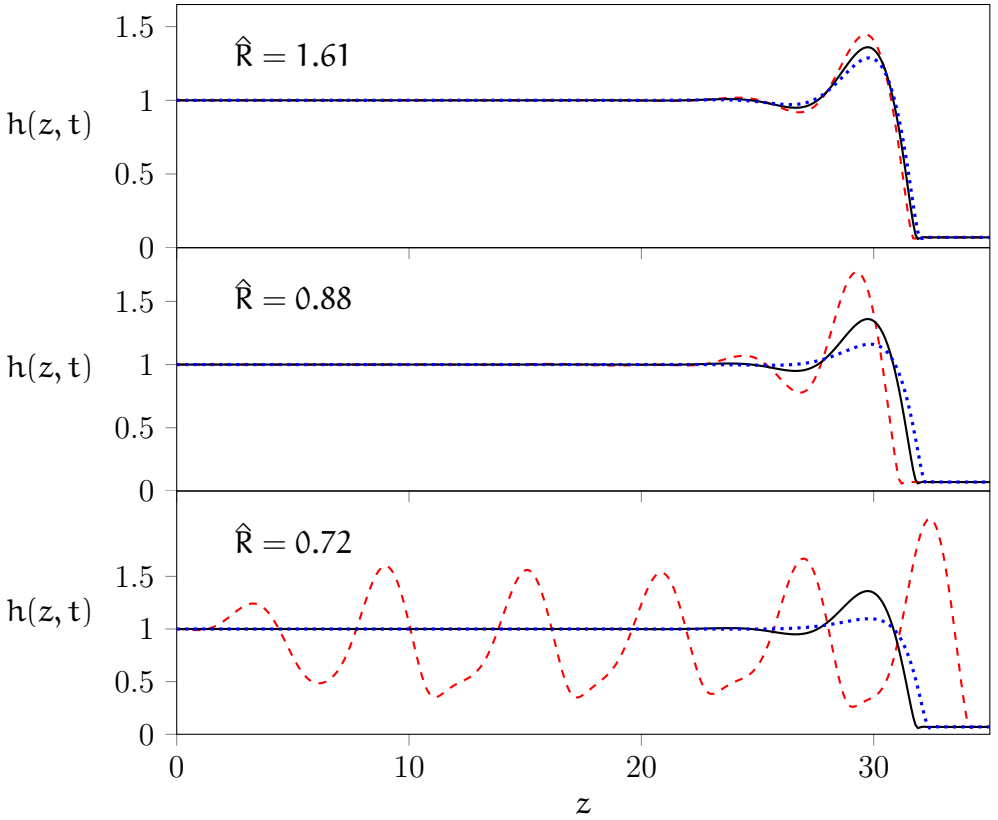
Figure 1: Two dimensional solutions of (7) for $\hat{R} = 1.61, 0.88, 0.72$ and $\beta = -1$ (blue dotted), $\beta = 0$ (black solid) and $\beta = 1$ (red dashed). These are each computed on a domain of 3501 nodes by allowing the fluid to evolve to dimensionless time $t = 22$.

and its presence is known to be a necessary condition for the instability of the flow [7]. In the middle plot, for the smaller radius $\hat{R} = 0.88$, the strengthening of the substrate curvature effect is evident as the three profiles vary in shape. The profile for flow down the outside of the cylinder ($\beta = 1$) possesses the largest capillary ridge, indicating the highest level of instability. In contrast, the small ridge for flow on the inside ($\beta = -1$) shows a low level of instability. The bottom plot, drawn for the radius $\hat{R} = 0.72$, illustrates a further destabilisation of the film down the outside of the cylinder ($\beta = 1$) in response to high substrate curvature. Here we observe a free surface wave instability which appears as a train of waves behind the leading capillary ridge [9, 12]. On the other hand, flow down the inside ($\beta = -1$) becomes even less unstable as substrate curvature increases, with the height of the capillary ridge diminishing as $\hat{R}$ decreases.

We now return to the full evolution equation (1) and simulate fingering instabilities at the advancing contact line of the film. The gravity driven process is inherently unstable, and so very small perturbations are imposed on the initial contact line to encourage the growth of fingers. The axisymmetric solution from (7) is taken as the base state for the unperturbed contact line, and then random perturbations are placed in the manner described by Kondic and Diez [7] to create the initial conditions for the following simulations. Mayo et al. [12] showed that substrate curvature has an insignificant effect on the flow for radii greater than $\hat{R} = 2.56$. Therefore, we are motivated to consider radii below this value in our numerical simulations.

In Figure 2 three dimensional simulations are shown for $\hat{R} = 1.53$ and $\beta = -1, 0, 1$. Each simulation was performed with the same initial condition and on an equivalently sized domain with periodic conditions on the lateral edges. They were allowed to evolve to dimensionless time $t = 100$. For flow down the outside of the cylinder ($\beta = 1$), the contour plot measuring $h(\theta, z)$ shows a long finger with a capillary ridge at the tip (indicated by the lightest shaded region). A finger is also present in the planar case with no substrate curvature ($\beta = 0$), but is significantly shorter. For flow down the inside of a cylinder ($\beta = -1$) there is only a slight perturbation visible at the contact
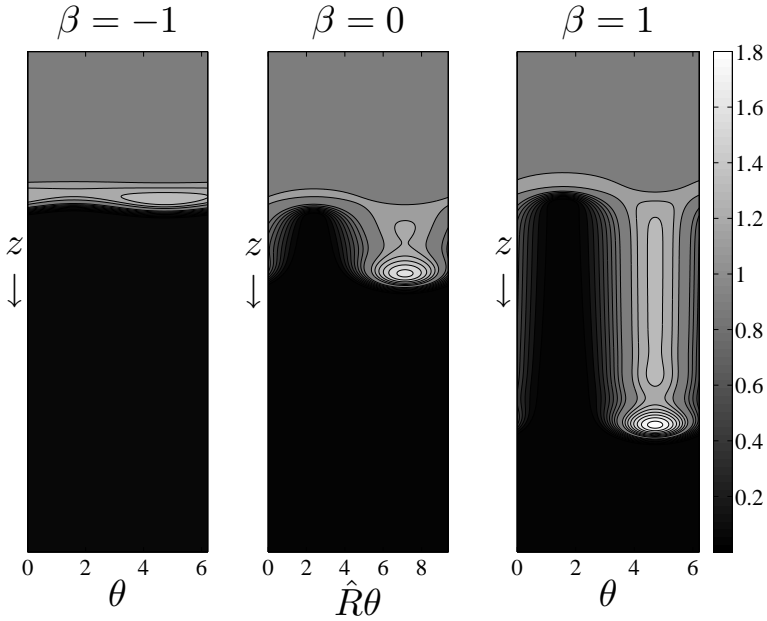
Figure 2: Solutions of (1) for $\hat{R} = 1.53$ and $\beta = -1, 0, 1$. Simulations evolved until dimensionless time $t = 100$ on a periodic domain of $112,894$ nodes. Grid spacing is $\Delta z = 0.05$, $\hat{R}\Delta\theta \approx 0.1$.

line. The lack of a finger for $\beta = -1$ indicates that flow down the inside is the least unstable to fingering of the three cases. A further reduction in the cylinder radius below roughly $\hat{R} = 1.53$ results in a completely stable contact line for flow down the inside of a cylinder ($\beta = -1$). In this case, all initial perturbations decay in time and the flow quickly becomes axisymmetric.

An interesting result is that we are able to observe 'nontrivial travelling waves' in our three dimensional solutions for flow down the inside of a cylinder ($\beta = -1$), as was documented for the analogous problem of flow down an inclined plane [8]. These travelling waves occur when the fingers at the contact line reach growth saturation, and the entire fingering pattern propagates at a constant speed without changing shape. This is in contrast to flow down a

vertical wall ($\beta = 0$), down the outside of a cylinder ($\beta = 1$), and down an inverted plane, for which the length of the fingers continue to grow for all time [7, 10, 12].

To illustrate these two features, Figure 3 shows the results of two simulations for a cylinder of radius $\hat{R} = 1.89$. The first row is for flow down the outside of the cylinder ($\beta = 1$) and the second for flow down the inside ($\beta = -1$). Solutions are shown at dimensionless times $t = 140, 220, 300$ and the same initial condition and domain size were used for each case. In the first row the finger on the outside of the cylinder continues to grow in length over the given time period. Running the simulations up to $t = 500$ showed that this growth continues. However, for flow down the inside of a cylinder, the second row illustrates that the growth rate of the finger saturates some time after $t = 140$, and the film forms a nontrivial travelling wave where the fluid front continues to propagate down the cylinder wall with the finger in a steady formation (recall that we are using a shifting computational window and so the values on the z axes in Figure 3 are present to indicate the distance the fluid front has moved over time). These nontrivial travelling waves become more difficult to observe as $\hat{R}$ increases (that is, as substrate curvature decreases) due to larger initial growth rates of the perturbations. Kondic and Diez [8] suggested, for their analogous problem of flow on an inclined plane, that growth saturation will eventually occur as long as the plane is inclined less than $\alpha = \pi/2$. Therefore, we may expect this phenomenon to occur in our simulations for all finite $\hat{R}$ while $\beta = -1$.

Simulations of (1) were performed for a larger range of $\hat{R}$ values than those presented in this report. However, Figures 1–3 are sufficient to capture the main results. For values of $\hat{R} \geqslant 1.53$, the same number and placement of fingers were consistently observed for the three cases $\beta = -1, 0, 1$, suggesting that the curvature has little effect on the preferred wavelength of the fingering pattern. Only the growth rate of the fingers was seen to change, indicating the difference in instability between the three cases. Linear stability analyses quantify these growth rates and relate them to the size of the initial perturbation [7, 10, 16]. While we presented simulations with only one finger, the

number of fingers increases approximately linearly with cylinder radius [12, 16]. However, it becomes more difficult to observe the effect of substrate curvature at larger radii. In summary, the two and three dimensional simulations both suggest that substrate curvature has the effect of increasing instability for flow down the outside of a cylinder, while for flow down the inside of a cylinder it has a stabilising effect.

4   Discussion

Mayo et al. [12] presented two and three dimensional numerical simulations for flow down the outside of a vertical cylinder. Good agreement was observed between those results and both the experimental observations and linear stability predictions of Smolka and SeGall [16]. Here we presented some preliminary results for the complementary regime of unstable flow down the inside of a vertical cylinder, which is analogous to the well studied problem of flow down an inclined plane.

When compared to the (intermediate) problem of flow down a vertical plane, the effect of substrate curvature on flow down the outside of a cylinder is to increase the instability of the flow to small perturbations at the contact line. For flow down the inside of the cylinder substrate curvature has the opposite effect. These findings are evident in both two dimensional simulations of the fluid profile and three dimensional simulations of the fingering patterns. Further, the number and form of fingers in the contact line does not change between the three cases; it is only their growth rates that differ. This effect is magnified at small radii, but becomes insignificant when the radius becomes reasonably large.

Our simulations demonstrate the existence of nontrivial travelling wave behaviour on the inside of a cylinder, in agreement with studies of flow down an inclined plane. This behaviour is not observed for the more unstable regimes of flow down a vertical plane or down the outside of the cylinder.
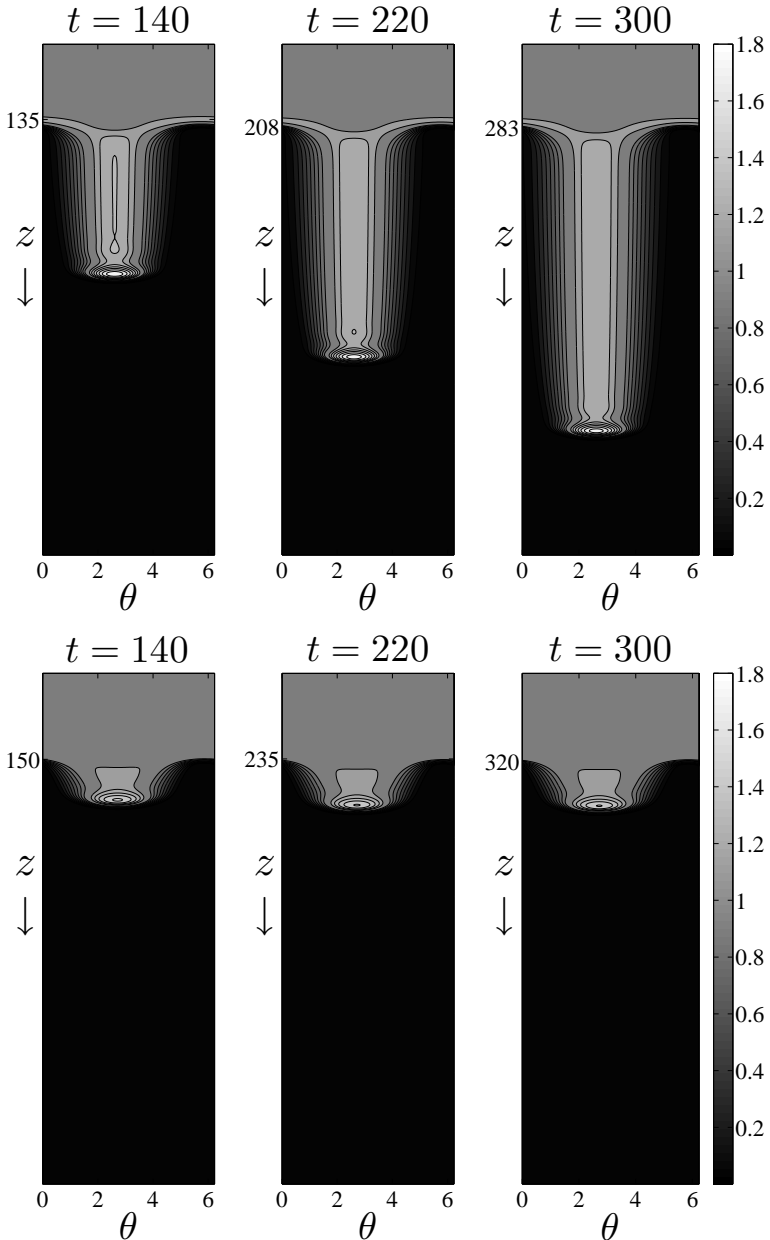
Figure 3: Solutions of (1) for $\hat{R} = 1.89$ and $\beta = 1$ (first row) and $\beta = -1$ (second row). Simulations evolved until dimensionless time $t = 300$ on a periodic domain of $306,918$ nodes. Grid spacing is $\Delta z = 0.05$, $\hat{R}\Delta\theta \approx 0.1$.

The ADI method used to solve the fourth order evolution equation is a powerful tool for producing efficient flow simulations. The non-iterative pseudolinear scheme employed here factorised the problem into a family of smaller one dimensional problems. At each time step, this required the solution of just two linear pentadiagonal systems. The review by Witleski and Bowen [19] offers several alternative ADI methods, some of which are second order in time. It may be worth investigating these for more accurate solutions of (1). An adaptive time stepping scheme may be of further benefit.

References

[1] A. L. Bertozzi and M. P. Brenner, Linear stability and transient growth in driven contact lines, *Phys. Fluids*, **9**:530–539, 1997. doi:10.1063/1.869217 C380

[2] R. V. Craster and O. K. Matar, Dynamics and stability of thin liquid films, *Rev. Mod. Phys.*, **81**:1131–1198, 2009. doi:10.1103/RevModPhys.81.1131 C378

[3] R. V. Craster and O. K. Matar, On viscous beads flowing down a vertical fibre, *J. Fluid Mech.*, **553**:85–105, 2006. doi:10.1017/S0022112006008706 C379

[4] L. M. Hocking, Spreading and instability of a viscous fluid sheet, *J. Fluid Mech.*, **211**:373–392, 1990. doi:10.1017/S0022112090001616 C380

[5] H. E. Huppert, Flow and instability of a viscous current down a slope, *Nature*, **300**:427–429, 1982. doi:10.1038/300427a0 C380

[6] I. L. Kliakhandler, S. H. Davis and S. G. Bankoff, Viscous beads on vertical fibre, *J. Fluid Mech.*, **429**:381–390, 2001. doi:10.1017/S0022112000003268 C379

[7] L. Kondic and J. Diez, Pattern formation in the flow of thin films down an incline: Constant flux configuration, *Phys. Fluids*, **13**:3168–3184, 2001. doi:10.1063/1.1409965 C378, C380, C385, C387

[8] L. Kondic and J. Diez, On nontrivial travelling waves in thin film flows including contact lines, *Physica D*, **209**:135–144, 2005. doi:10.1016/j.physd.2005.06.029 C386, C387

[9] T.-S. Lin and L. Kondic, Thin films flowing down inverted substrates: Two dimensional flow, *Phys. Fluids*, **22**:052105, 2010. doi:10.1063/1.3428753 C379, C385

[10] T.-S. Lin, L. Kondic and A. Filippov, Thin films flowing down inverted substrates: Three dimensional flow, *Phys. Fluids*, **24**:022105, 2012. doi:10.1063/1.3682001 C379, C381, C387

[11] J. R. Lister, J. M. Rallison and S. J. Rees, The nonlinear dynamics of pendent drops on a thin film coating the underside of a ceiling, *J. Fluid Mech.*, **647**:239–264, 2010. doi:10.1017/S002211201000008X C381

[12] L. C. Mayo, S. W. McCue and T. J. Moroney, Gravity-driven fingering simulations for a thin liquid film flowing down the outside of a vertical cylinder, *Phys. Rev. E*, **87**:053018, 2013. doi:10.1103/PhysRevE.87.053018. C379, C380, C382, C383, C385, C387, C388

[13] T. G. Myers, Thin films with high surface tension, *SIAM Rev.*, **40**:441–462, 1998. doi:10.1137/S003614459529284X C378

[14] A. Oron, S. H. Davis and S. G. Bankoff, Long-scale evolution of thin liquid films, *Rev. Mod. Phys.*, **69**:931–980, 1997. doi:10.1103/RevModPhys.69.931 C378

[15] W. H. Press, S. A. Teukolsky, W. T. Vetterling and B. P Flannery, *Numerical Recipes in C* 2nd ed., Cambridge University Press, Chap. 2, Sec. 7, 1992. C383

[16] L. B. Smolka and M. SeGall, Fingering instability down the outside of a vertical cylinder, *Phys. Fluids*, **23**:092103, 2011. doi:10.1063/1.3633530 C379, C387, C388

[17] L. W. Schwartz, Hysteretic effects in droplet motions on heterogeneous substrates: Direct numerical simulation, *Langmuir*, **14**:3440–3453, 1998. doi:10.1021/la971407t C381

[18] S. M. Troian, E. Herbolzheimers, A. Safran and J. F. Joanny, Fingering instabilities of driven spreading films, *Europhys. Lett.*, **10**:25–30, 1989. doi:10.1209/0295-5075/10/1/005 C380

[19] T. P. Witelski and M. Bowen, ADI schemes for higher-order nonlinear diffusion equations, *Appl. Numer. Math.*, **45**:331–351, 2003. doi:10.1016/S0168-9274(02)00194-0 C381, C382, C390

Author addresses

1. **Lisa C. Mayo**, Mathematical Sciences, Queensland University of Technology, Brisbane QLD 4001, Australia.
   mailto:lisa.mayo@student.qut.edu.au

2. **Scott W. McCue**, Mathematical Sciences, Queensland University of Technology, Brisbane QLD 4001, Australia.
   mailto:scott.mccue@qut.edu.au

3. **Timothy J. Moroney**, Mathematical Sciences, Queensland University of Technology, Brisbane QLD 4001, Australia.
mailto:t.moroney@qut.edu.au